Tracer Conservation and Local Consistency for Three-Dimensional, Finite Element, Free-Surface Ocean Modeling on Moving Prismatic Meshes*

Laurent White[1,2]†, Vincent Legat[1], Eric Deleersnijder[2,1]

March 25, 2007

[1]Université catholique de Louvain
Centre for Systems Engineering and Applied Mechanics (CESAME)
4, Avenue G. Lemaître, B-1348 Louvain-la-Neuve, Belgium

[2]Université catholique de Louvain
G. Lemaître Institute of Astronomy and Geophysics (ASTR)
2, Chemin du Cyclotron, B-1348 Louvain-la-Neuve, Belgium

Abstract

Large-scale free-surface ocean models designed to run over climatic timescales are required to globally conserve the volume and any tracer up to machine precision. In addition, the following property is critical. Setting a tracer concentration to a uniform value throughout the closed domain and letting the free surface undulate, the same tracer concentration must be recovered at any later time if there is no tracer source. This property of consistency, together with monotonicity, will ensure that no spurious tracer extrema occur. A three-dimensional, finite-element, shallow-water model is presented. The model consistently conserves any tracer globally. The mesh is unstructured in the horizontal, extruded in the third dimension and made up of prisms. In addition, the mesh is allowed to move in the vertical and accommodates the free-surface motions. It is shown that achieving consistency requires a discrete compatibility between the tracer and continuity equations. In addition, to ensure global tracer conservation in a consistent way, a discrete compatibility between the tracer, continuity and free-surface equations must be fulfilled. It is suggested that this compatibility constraint, together with the use of a numerically stable scheme, severely restricts the choice of usable finite element spatial discretizations. Some illustrative test cases are presented where the method is shown to satisfy all conservation properties. A few experiments where consistency breaks down are carried out and the consequences of it investigated.

1 Introduction

The intrinsic flexibility of unstructured meshes is compelling for numerical ocean modeling. Complex topographic features, such as coastlines, islands, narrow straits and sills, can faithfully be represented by locally increasing the mesh resolution and because there is no constraint on the mesh topology (e.g., Legrand et al., 2006). The resolution can also be altered based upon other criteria such as that based on the bathymetry (Gorman et al., 2006; Legrand et al., accepted) or a model variable (Legrand et al., 2000). In the latter case, the mesh can also be dynamically adapted in the course of the simulation (Piggott et al., 2005; Power et al., 2006). Over the last decade, motivated by these concepts, there has been increasing effort into the development of marine models based on unstructured meshes. Three classes of numerical methods can readily handle unstructured meshes: the finite volume (FV), the spectral element (SE) and the finite element (FE) methods.

To a certain extent, each of these methods has been gaining popularity in the ocean modeling community. For example, the finite volume method is employed by Casulli and Walters (2000), Ham et al. (2005) and Fringer et al. (2006). The SE method is used by Iskandarani et al. (1995) and Iskandarani et al. (2003). The use of the FE method for coastal, shelf and estuarine areas started somewhat earlier (Lynch and Werner, 1987; Walters and Werner, 1989; Lynch and Werner, 1991). During the nineties,

*Revised version submitted to Monthly Weather Review on March ??, 2007.
†Corresponding author. E-mail: lwhite@mema.ucl.ac.be, Tel: +32 10 47 23 57, Fax: +32 10 47 21 80

aside from some results obtained with diagnostic finite element ocean models (Myers and Weaver, 1995; Greenberg et al., 1998), we did not really see any revolutionary change. Over the last five years, with new projects of finite element global ocean models, such as FEOM (Finite Element Ocean circulation Model) from the Alfred Wegener Institude for Polar and Marine Research, ICOM (Imperial College Ocean Model) from Imperial College and SLIM (Second-generation Louvain-la-Neuve Ice-ocean Model) from Université catholique de Louvain, we have been witnessing a new wave of thriving development (and funding) of prognostic finite element ocean models. As warranted by the literature, the FE method appears to be the most promising (e.g., Pietrzak et al., 2005, 2006). There might be two main reasons for this. All the methods mentioned can handle unstructured meshes indeed but the finite element method offers additional flexibility in the choice of interpolation (it can be of low or high order and continuous or discontinuous) and is sustained by a rigorous mathematical framework, in which a priori and a posteriori error estimates can be established.

The first developments of finite element marine models were based on the wave continuity equation (Lynch and Gray, 1979), whereby the primitive shallow-water equations are manipulated to form a wave equation for the free-surface elevation. This formulation does not suffer from spurious oscillations occurring when using the primitive equations and the same interpolation for the velocity and the elevation. The generalization of the original method led to the generalized wave continuity equation (GWCE), documented by Kinnmark (1986) and Kolar et al. (1994). The GWCE has been extensively used over the past 20 years with successful applications in coastal regions for tidal predictions (Walters, 1992; Lynch and Naimie, 1993; Lynch et al., 1996; Fortunato et al., 1997; Cushman-Roisin and Naimie, 2002). Despite these encouraging applications and the ongoing research to improve the method, it remains plagued by two caveats. GWCE-based models are subject to advective instabilities (Kolar et al., 1994) and the GWCE form sacrifices the primitive continuity equation, thus the primitive form is no longer satisfied in a discrete sense, which implies continuity (or mass) imbalances (Dawson et al., 2006; Massey and Blain, 2006), rendering the method less suitable for coupling with transport equations, let alone for long time integrations (more than several years) in which conservation is crucial.

Since the end of the nineties, more efforts have been directed towards finding a mixed finite element pair for the primitive shallow-water equations that does not support spurious oscillations (Le Roux et al., 1998). Aware of the limitations of the GWCE and urged to develop primitive equations finite element ocean models, research towards this goal intensified (Le Roux, 2001; Hanert and Deleersnijder, 2003; Le Roux, 2005; Le Roux et al., 2005; Walters, 2006; White et al., 2006b; Le Roux et al., in press). Early issues of the method often cited as reasons not to use it – such as spurious oscillations, unphysical wave scattering due to the unstructured character of the mesh and lack of mass conservation – are starting to wither. Nowadays, applications of FE shallow-water models based on the primitive equations are becoming much less of an exception (Nechaev et al., 2003; Danilov et al., 2004; Ford et al., 2004a,b; Pain et al., 2004; Danilov et al., 2005; Hanert et al., 2005; Labeur and Pietrzak, 2005; Walters, 2006; White et al., 2006a; White and Deleersnijder, in press; White et al., submitted) and this trend is unlikely to lose its momentum.

Finite element methods based on the primitive equations encompass both the continuous Galerkin (CG) and discontinuous Galerkin (DG) methods. The latter applied to the shallow-water equations is newer than the former and has much to offer for solving hyperbolic systems of equation (Flaherty et al., 2002) and advection-dominated flows in general (e.g., Hanert et al., 2004; Kubatko et al., 2006a). Furthermore, the method is known to conserve flow properties elementwise in the intuitive meaning of the FV method (as opposed to the local conservation property of CG methods described by Hughes et al. (2000)). At least for now, DG methods remain less mature than CG methods for ocean modeling. They have nonetheless been gaining popularity for modeling shallow-water flows as well (Schwanenberg et al., 2000; Aizinger and Dawson, 2002; Schwanenberg and Harms, 2004; Nair et al., 2005; Kubatko et al., 2006a; White et al., 2006b; Bernard et al., accepted) and are particularly well suited for transport problems (Kubatko et al., 2006b).

Despite these recent achievements, many challenges still lie ahead of us. Admittedly, switching from structured meshes to unstructured meshes requires developers to build new models from scratch rather than converting existing ones piece by piece. Quite ironically, with this approach, we find ourselves in need of addressing issues that have been solved in finite difference (FD) models but that remain somewhat problematic or controversial with finite element models. Ensuring global tracer conservation while preserving consistency (i.e., compatibility) between equations in finite element shallow-water models is one of these issues and the core of this paper. This very issue has already been thoroughly addressed in FD models (Deleersnijder, 1993; Roullet and Madec, 2000; Griffies et al., 2001; Campin et al., 2004; Griffies, 2004). A common deceitful criticism of the CG method is the lack of elementwise conservation. Several attempts at proving those criticisms wrong have been made by defining interelement fluxes appropriately

using so-called nodal fluxes (Hughes et al., 2000; Berger and Howington, 2002). Those efforts, however, have not really mitigated the widespread belief that the finite element method is not conservative and, thereby, not suitable for ocean modeling. In this paper, we demonstrate how to achieve global tracer conservation and consistency in a three-dimensional, free-surface, FE shallow-water model on moving meshes. The model, whose description and validation are presented by White et al. (submitted), solves the hydrostatic primitive equations and conserves mass and tracers globally. Global tracer conservation is attained if the volume integral of any tracer concentration within the domain is fixed in time, in the absence of boundary fluxes and source terms. It is unquestionable to us that any ocean model aimed at running over climatic timescales must achieve global conservation. Consistency or compatibility is meant in the following sense: in a discrete model, set a tracer concentration to a uniform value throughout the domain and let the free surface undulate, yet do not add boundary fluxes; the tracer concentration must maintain the same uniform value at all time. If this property is not satisfied, artificial tracer extrema might appear with the indirect effect of generating unphysical currents (in case the tracer is temperature or salinity). For this reason, it is indispensable that any ocean model solve the elevation, continuity and tracer equations in a consistent way. That is, they must be discretely compatible. Note that in FD models, consistency is commonly referred to as local conservation (Griffies et al., 2001; Campin et al., 2004; Griffies, 2004). This is so because ensuring conservation at the cell level in terms of fluxes does imply consistency. This is no necessarily true in FE models where the scheme could be locally conservative in terms of nodal fluxes without solving the equations consistently. In addition to these properties, we opted for a free-surface formulation. Rigid-lid formulations are now deemed obsolete for several reasons (Killworth et al., 1991; Deleersnijder and Campin, 1995; Griffies et al., 2000), one of them being the inability to easily account for surface freshwater fluxes. Finally, the domain is time-dependent to accommodate free-surface motions. All layers within the domain are free to move in the vertical so that the free-surface displacement is distributed over the vertical to avoid the occurrence of overly thin layers near the surface. As will be shown, the volume change due to freshwater input (output) automatically leads to dilution (concentration) of salt without having to resort to salt fluxes.

In this paper, we derive sufficient conditions regarding the FE spatial discretization to ensure global tracer conservation and consistency. We show that the same interpolation in the horizontal must be used for the elevation, the vertical velocity and the tracers. Moreover, the same interpolation in the vertical must be used for the vertical velocity and the tracers. It is also demonstrated that computing the vertical velocity via the continuity equation, integrating it upwards or downwards and subject to one boundary condition, is well posed and does not lead to any accumulation of errors as was earlier suggested (Lynch and Naimie, 1993; Muccino et al., 1997; Danilov et al., 2004). This remains true as long as the upper boundary of the domain coincides with the free surface and a consistent horizontal velocity is used. Some illustrative test cases are presented where the method is shown to satisfy all conservation properties. We also carry out a few experiments where consistency breaks down and investigate the consequences therefrom. We hope that this paper will successfully address some of the misunderstandings between traditional ocean modelers and those scientists willing to apply finite element methods to geophysical flow problems.

2 Mathematical formulation

We shall now describe the minimum set of equations needed in our study. In this section, all classical conservation properties are inferred from the continuous equations. In section 3, we will derive a set of conditions for which these properties carry over to the discrete equations. Let $\Omega(t)$ be the three-dimensional, time-dependent domain of interest. It is bounded below by the seabed, defined by Γ_b and above by the free surface, defined by Γ_s, as depicted in Figure (1). The seabed is considered time-independent. The free surface, on the other hand, is time-dependent. The lateral boundary, defined by Γ_n, is parallel to the z-direction and has a constant (x, y)-position. For simplicity, we do not consider open boundaries in this work. The domain boundary can thus be written as $\partial\Omega = \Gamma_n \cup \Gamma_b \cup \Gamma_s$. The unperturbed surface defined by $z = 0$ is noted $\mathcal{T}$. We work within the scope of the Boussinesq and hydrostatic approximations.

2.1 Equations and boundary conditions

Let $\mathbf{u}(x, y, z, t) = (u(x, y, z, t); v(x, y, z, t))$ be the horizontal velocity, with components u and v in the x and y directions, respectively. The vertical velocity is the component in the z direction and is denoted by $w(x, y, z, t)$. The free-surface elevation $\eta(x, y, t)$ does not depend on z and is defined with respect to the reference level $\mathcal{T}$. The unperturbed depth $d(x, y)$, also defined with respect to $\mathcal{T}$, is assumed to be

time-independent, does not depend on z and is everywhere nonnegative. The layer thickness, H, is the sum of the depth and the free-surface elevation: $H(x, y, t) = d(x, y) + \eta(x, y, t)$. With those notations, the lower and upper domain boundaries are characterized by $\Gamma_b \equiv z = -d$ and $\Gamma_s \equiv z = \eta$.

For the purpose of deriving the statements of volume and tracer conservation, there is no need to write out the full horizontal momentum equations. We simply assume that the horizontal velocity $\mathbf{u}$ is known in $\Omega(t)$ and that it satisfies the impermeability condition on the lateral boundary Γ_n, that is

$$\mathbf{u} \cdot \mathbf{n} = 0 \qquad \text{on } \Gamma_n, \tag{1}$$

where $\mathbf{n} = (n_x, n_y)$ is the unit outward-pointing normal to Γ_n. We will also note n_z the vertical component of the normal. In hydrostatic models, the vertical momentum equation reduces to hydrostatic equilibrium. Hence, there is no prognostic equation for the vertical velocity. The latter is computed diagnostically via the continuity equation

$$\boldsymbol{\nabla} \cdot \mathbf{u} + \frac{\partial w}{\partial z} = 0 \qquad \text{in } \Omega, \tag{2}$$

where $\boldsymbol{\nabla}$ is the horizontal gradient operator. Eq. (2) is a statement of volume conservation. Another statement of volume conservation is obtained by depth-integrating Eq. (2). This yields the following prognostic equation for the free-surface elevation:

$$\frac{\partial \eta}{\partial t} + \boldsymbol{\nabla} \cdot \int_{-d}^{\eta} \mathbf{u} \, \mathrm{d}z = q_w \qquad \text{on } \mathcal{T}, \tag{3}$$

for which use has been made of the impermeability of the seabed and the free surface. These impermeability conditions (the so-called kinematic boundary conditions) read

$$w = -\mathbf{u} \cdot \boldsymbol{\nabla} d \qquad \text{on } \Gamma_b, \tag{4}$$

$$w = \frac{\partial \eta}{\partial t} + \mathbf{u} \cdot \boldsymbol{\nabla} \eta - q_w \qquad \text{on } \Gamma_s, \tag{5}$$

where q_w is the net freshwater volume flux per unit area (with units of a velocity) due to precipitation ($q_w > 0$), evaporation ($q_w < 0$) and river runoffs ($q_w > 0$), if the latter are not formulated as lateral boundary conditions. Note that boundary conditions (4) and (5) can also be written as

$$\mathbf{u} \cdot \mathbf{n} + w n_z = 0 \qquad \text{on } \Gamma_b, \tag{6}$$

$$\mathbf{u} \cdot \mathbf{n} + w n_z = \left(\frac{\partial \eta}{\partial t} - q_w \right) n_z \qquad \text{on } \Gamma_s, \tag{7}$$

where we assume that the orientation of the freshwater flux is the same as that associated with the normal at the free surface. Finally, a given tracer with concentration C obeys an advection-diffusion equation (with no source term) of the form

$$\frac{\partial C}{\partial t} + \boldsymbol{\nabla} \cdot (\mathbf{u} C) + \frac{\partial \left(w C \right)}{\partial z} = \boldsymbol{\nabla} \cdot (\kappa \boldsymbol{\nabla} C) + \frac{\partial}{\partial z} \left(\kappa \frac{\partial C}{\partial z} \right) \qquad \text{in } \Omega, \tag{8}$$

where κ is the eddy diffusivity coefficient. A condition of no diffusive flux is prescribed at the boundary:

$$\kappa \frac{\partial C}{\partial n} = 0 \qquad \text{on } \partial\Omega, \tag{9}$$

where $\frac{\partial C}{\partial n}$ is the normal derivative.

2.2 Conservation properties

From the equations presented above, we may now derive the statements of volume and tracer conservation and check the consistency between the tracer and continuity equations. For simplicity, the freshwater flux is set to zero, $q_w = 0$.

2.2.1 Volume conservation

By integrating Eq. (3) over the time-independent, two-dimensional domain $\mathcal{T}$ and using the divergence theorem to compute the second integral, we obtain

$$\int_{\mathcal{T}} \frac{\partial \eta}{\partial t} \, \mathrm{d}\mathcal{T} + \int_{\Gamma_n} \mathbf{u} \cdot \mathbf{n} \, \mathrm{d}\Gamma = 0,$$

which, by using the boundary condition (1), further reduces to

$$\frac{\mathrm{d}}{\mathrm{d}t}\int_{\mathcal{T}} \eta \; \mathrm{d}\mathcal{T} = 0. \tag{10}$$

Eq. (10) is the statement of volume conservation.

2.2.2 Global tracer conservation

Integrating Eq. (8) over $\Omega(t)$, using the divergence theorem for the advection and diffusion terms and enforcing the boundary condition (9) leads to

$$\int_{\Omega(t)} \frac{\partial C}{\partial t} \; \mathrm{d}\Omega + \int_{\Gamma_n} \mathbf{u}\cdot\mathbf{n}\, C \; \mathrm{d}\Gamma + \int_{\Gamma_b} (\mathbf{u}\cdot\mathbf{n} + w n_z)\, C \; \mathrm{d}\Gamma + \int_{\Gamma_s} (\mathbf{u}\cdot\mathbf{n} + w n_z)\, C \; \mathrm{d}\Gamma = 0. \tag{11}$$

The integrals over Γ_n and Γ_b vanish by enforcing boundary conditions (1) and (6). Using the Reynolds transport theorem, the first term of the expression above becomes

$$\int_{\Omega(t)} \frac{\partial C}{\partial t} \; \mathrm{d}\Omega = \frac{\mathrm{d}}{\mathrm{d}t}\int_{\Omega(t)} C \; \mathrm{d}\Omega - \int_{\Gamma_s} C \frac{\partial \eta}{\partial t} n_z \; \mathrm{d}\Gamma,$$

with the velocity of the moving boundary Γ_s being equal to that of the free surface. Eq. (11) becomes

$$\frac{\mathrm{d}}{\mathrm{d}t}\int_{\Omega(t)} C \; \mathrm{d}\Omega + \int_{\Gamma_s} \left(\mathbf{u}\cdot\mathbf{n} + w n_z - \frac{\partial \eta}{\partial t} n_z\right) C \; \mathrm{d}\Gamma = 0.$$

Now, using boundary condition (7) yields the statement of global tracer conservation:

$$\frac{\mathrm{d}}{\mathrm{d}t}\int_{\Omega(t)} C \; \mathrm{d}\Omega = 0. \tag{12}$$

2.2.3 Consistency

The property of consistency is equivalent to verifying that a constant tracer concentration is solution to (8)-(9). Setting $C = C_0 \neq 0$ in Eq. (8), C_0 being a constant, we simply obtain

$$C_0 \left(\boldsymbol{\nabla}\cdot\mathbf{u} + \frac{\partial w}{\partial z}\right) = 0 \qquad \text{in } \Omega.$$

Therefore, the continuity and tracer equations are consistent (or compatible) with each other when the following relation holds true

$$C_0 \left(\boldsymbol{\nabla}\cdot\mathbf{u} + \frac{\partial w}{\partial z}\right) = 0 \iff \boldsymbol{\nabla}\cdot\mathbf{u} + \frac{\partial w}{\partial z} = 0 \qquad \text{in } \Omega \text{ and for } C_0 \neq 0. \tag{13}$$

3 The discrete conservation laws

The purpose of this section is to derive the discrete counterparts of Eqs (10), (12) and (13). We start by describing the mesh topology and introducing a few useful notations. We then present the variational formulations of the elevation, continuity and tracer equations, followed by their discretization based upon the Galerkin procedure. The discrete conservation laws will then be inferred from the discrete equations. In order to keep notations more concise, all subsequent developments are carried out for the CG method.

3.1 Mesh topology

The numerical solution is sought in the three-dimensional domain Ω^h. The latter consists of an approximation of the physical domain, obtained by interpolating the boundaries of topographical features and the bathymetry. Within this framework, all boundaries are also interpolated so that we have $\partial\Omega \simeq \partial\Omega^h = \Gamma_b^h \cup \Gamma_s^h \cup \Gamma_n^h$. The three-dimensional finite element mesh (Figure 2) is obtained by first partitioning $\mathcal{T}^h$ into N_t open non-overlapping triangles $\mathcal{T}_e$. Extrusion of each triangle $\mathcal{T}_e$ into a prismatic column is then performed so as to exactly fit the sea bottom Γ_b^h and the free surface Γ_s^h. The domain Ω^h is naturally partitioned by splitting up each column into prisms Ω_e.

3.2 Variational statements

The variational statements involve integrations over geometrical items in two and three dimensions. The following notations are used:

$$\int \square \, d\Omega: \quad \text{3D integration over prisms,}$$

$$\int \square \, d\Gamma: \quad \text{2D integration over rectangular faces (vertical faces),}$$

$$\int \square \, d\tau: \quad \text{2D integration over triangular faces.}$$

3.2.1 Free-surface elevation equation

For the free-surface equation (3), the variational statement at any given time t consists in finding $\eta(x, y, t) \in \mathcal{H}$ such that

$$\int_{\mathcal{T}^h} \left[\frac{\partial \eta}{\partial t} + \boldsymbol{\nabla} \cdot \left(\int_{-d}^{\eta} \mathbf{u} \, \mathrm{d}z \right) \right] \hat{\eta} \, \mathrm{d}\tau = 0 \quad \forall \, \hat{\eta} \in \mathcal{H}, \tag{14}$$

where $\mathcal{H}$ is a suitable functional space. Integrating the divergence term by parts leads to

$$\int_{\mathcal{T}^h} \left[\frac{\partial \eta}{\partial t} \hat{\eta} - \left(\int_{-d}^{\eta} \mathbf{u} \, \mathrm{d}z \right) \cdot \boldsymbol{\nabla} \hat{\eta} \right] \mathrm{d}\tau + \int_{\Gamma_n^h} \mathbf{u} \cdot \mathbf{n} \, \hat{\eta} \, \mathrm{d}\Gamma = 0. \quad \forall \, \hat{\eta} \in \mathcal{H},$$

By using the fact that $\boldsymbol{\nabla} \hat{\eta}$ is independent of z and by enforcing the impermeability condition (1), the above expression reduces to

$$\int_{\mathcal{T}^h} \frac{\partial \eta}{\partial t} \hat{\eta} \, \mathrm{d}\tau - \int_{\Omega^h} \mathbf{u} \cdot \boldsymbol{\nabla} \hat{\eta} \, \mathrm{d}\Omega = 0 \quad \forall \, \hat{\eta} \in \mathcal{H}. \tag{15}$$

3.2.2 Continuity equation

For the continuity equation, the variational statement at any given time t consists in finding $w(x, y, z, t) \in \mathcal{W}$ such that

$$\int_{\Omega^h} \left(\boldsymbol{\nabla} \cdot \mathbf{u} + \frac{\partial w}{\partial z} \right) \hat{w} \, \mathrm{d}\Omega = 0 \quad \forall \, \hat{w} \in \mathcal{W}, \tag{16}$$

where $\mathcal{W}$ is another suitable functional space. By integrating the above expression by parts, we obtain

$$- \int_{\Omega^h} \left(\mathbf{u} \cdot \boldsymbol{\nabla} \hat{w} + w \frac{\partial \hat{w}}{\partial z} \right) \mathrm{d}\Omega + \underbrace{\int_{\Gamma_n^h} \hat{w} \, \mathbf{u} \cdot \mathbf{n} \, \mathrm{d}\Gamma}_{1} + \underbrace{\int_{\Gamma_b^h} \hat{w} \, (\mathbf{u} \cdot \mathbf{n} + w n_z) \, \mathrm{d}\tau}_{2}$$

$$+ \underbrace{\int_{\Gamma_s^h} \hat{w} \, (\mathbf{u} \cdot \mathbf{n} + w n_z) \, \mathrm{d}\tau}_{3} = 0 \quad \forall \, \hat{w} \in \mathcal{W}.$$

A closer look at the terms labeled 1 to 3 will shed light on their meaning. By enforcing the impermeability condition of the lateral boundary and the seabed, namely conditions (1) and (6), integrals 1 and 2 vanish. Integral 3 does not vanish and must be computed in order to determine the vertical velocity on Γ_s^h. Note that the boundary condition (6) at the seabed is a natural boundary condition that is automatically incorporated into the variational statement. The continuity equation must then be integrated from the seabed upwards. This can be done by using upwind-biased test functions for the CG method or upwind-biased fluxes for the DG method. In an intuitive interpretation, the continuity equation can be viewed as a steady-state advection equation (with the advective velocity equal to one) with source term (the horizontal velocity divergence), which might help clarify the approach described above. We end up with the following variational statement:

$$- \int_{\Omega^h} \left(\mathbf{u} \cdot \boldsymbol{\nabla} \hat{w} + w \frac{\partial \hat{w}}{\partial z} \right) \mathrm{d}\Omega + \int_{\Gamma_s^h} \hat{w} \, (\mathbf{u} \cdot \mathbf{n} + w n_z) \, \mathrm{d}\tau = 0 \quad \forall \, \hat{w} \in \mathcal{W}. \tag{17}$$

3.2.3 Tracer equation

We now turn our attention to the tracer equation (8). Since the domain of integration Ω^h is time-dependent and a time derivative appears in Eq. (8), a little more work is needed prior to deriving the variational statement. We will recast the original equation into the so-called arbitrary Lagrangian-Eulerian (ALE) form. With this formulation, the mesh is neither fixed in space, nor does it follow the fluid. It is therefore neither Eulerian nor Lagrangian. A good review of ALE methods is presented by Donea et al. (2004). Following Farhat et al. (2001), we define a reference fixed mesh Ω_0^h and a mapping function $\mathbf{x}$ between Ω_0^h and Ω^h:

$$\mathcal{A} : \Omega_0^h \rightarrow \Omega^h : \boldsymbol{\xi} \rightarrow \mathcal{A}\left(\boldsymbol{\xi}, t\right) = \mathbf{x}.$$

This mapping simply associates a three-dimensional coordinate $\boldsymbol{\xi}$ of the reference mesh Ω_0^h to a three-dimensional coordinate $\mathbf{x} = (x, y, z)$ in the physical moving mesh Ω^h. We further assume that this transformation is invertible:

$$J = \left(\frac{\partial \mathbf{x}}{\partial \boldsymbol{\xi}}\right) > 0,$$

where J is the Jacobian of the transformation. We also require that the mapping associate the boundary of the reference mesh to the boundary of the physical mesh, i.e., $\mathcal{A}(\partial\Omega_0^h) = \partial\Omega^h$ without any other constraint on interior coordinates aside from some smoothness requirement. The conservative ALE form of Eq. (8) then reads (Formaggia and Nobile, 2004):

$$\frac{\partial (JC)}{\partial t}\Big|_{\xi} + J\boldsymbol{\nabla} \cdot (\mathbf{u}C) + J\frac{\partial \left(\tilde{w}C\right)}{\partial z} = J\boldsymbol{\nabla} \cdot (\kappa \boldsymbol{\nabla} C) + J\frac{\partial}{\partial z}\left(\kappa \frac{\partial C}{\partial z}\right) \quad \text{in } \Omega_0^h \tag{18}$$

where all terms are computed in the reference domain Ω_0^h. In particular, the time derivative is computed with respect to a fixed position in Ω_0^h. We have defined $\tilde{w} = w - w_m$, with the mesh velocity w_m given by

$$w_m = \frac{\partial z}{\partial t}\Big|_{\xi}.$$

With the presence of the mesh velocity, vertical advection is taken relative to the moving mesh. The variational statement for the tracer equation is obtained by multiplying Eq. (18) by a test function $\hat{C}$, integrating the result over the reference mesh and using the fact that $\mathrm{d}\Omega = J\mathrm{d}\Omega_0$. We seek $C \in \mathcal{G}$ such that

$$\begin{aligned} &\frac{\mathrm{d}}{\mathrm{d}t}\int_{\Omega^h(t)} C\hat{C}\ \mathrm{d}\Omega + \int_{\Omega^h(t)} \left[\boldsymbol{\nabla} \cdot (\mathbf{u}C) + \frac{\partial \left(\tilde{w}C\right)}{\partial z}\right]\hat{C}\ \mathrm{d}\Omega = \\ &\int_{\Omega^h(t)} \left[\boldsymbol{\nabla} \cdot (\kappa \boldsymbol{\nabla} C) + \frac{\partial}{\partial z}\left(\kappa \frac{\partial C}{\partial z}\right)\right]\hat{C}\ \mathrm{d}\Omega \quad \forall\, \hat{C} \in \mathcal{G}, \end{aligned} \tag{19}$$

where $\mathcal{G}$ is an appropriate functional space. The first term in the above expression was obtained by using the following result:

$$\int_{\Omega_0^h} \frac{\partial (JC)}{\partial t}\Big|_{\xi} \hat{C}\ \mathrm{d}\Omega_0 = \frac{\mathrm{d}}{\mathrm{d}t}\int_{\Omega_0^h} JC\hat{C}\ \mathrm{d}\Omega_0 = \frac{\mathrm{d}}{\mathrm{d}t}\int_{\Omega^h(t)} C\hat{C}\ \mathrm{d}\Omega,$$

where we used the fact that the test function does not depend on time in the reference mesh. It does, however, depend on time in the physical domain Ω^h. The advection and diffusion terms can be integrated by parts, which yields

$$\begin{aligned} &\int_{\Omega^h(t)} \left[\boldsymbol{\nabla} \cdot (\mathbf{u}C) + \frac{\partial \left(\tilde{w}C\right)}{\partial z}\right]\hat{C}\ \mathrm{d}\Omega = -\int_{\Omega^h(t)} C\left(\mathbf{u} \cdot \boldsymbol{\nabla}\hat{C} + \tilde{w}\frac{\partial \hat{C}}{\partial z}\right)\ \mathrm{d}\Omega \\ &+ \int_{\Gamma_s^h} C\hat{C}\left(\mathbf{u} \cdot \mathbf{n} + \tilde{w}n_z\right)\mathrm{d}\tau \end{aligned} \tag{20}$$

and

$$\int_{\Omega^h(t)} \left[\boldsymbol{\nabla} \cdot (\kappa \boldsymbol{\nabla} C) + \frac{\partial}{\partial z}\left(\kappa \frac{\partial C}{\partial z}\right)\right]\hat{C}\ \mathrm{d}\Omega = -\int_{\Omega^h(t)} \kappa\left(\boldsymbol{\nabla}\hat{C} \cdot \boldsymbol{\nabla} C + \frac{\partial \hat{C}}{\partial z}\frac{\partial C}{\partial z}\right)\mathrm{d}\Omega, \tag{21}$$

where we used the no-flux conditions (1), (6) and (9). Note that the right-hand side of Eq. (20) is nothing but the variational statement of the continuity equation (see Eq. 17) in which the velocity is multiplied by the tracer concentration C, the test function $\hat{w}$ is replaced by $\hat{C}$ and the modified vertical

velocity $\tilde{w}$ is used in place of the vertical velocity w. Now, using Eq. (20) and Eq. (21) in Eq. (19) gives rise to

$$\begin{aligned}&\frac{\mathrm{d}}{\mathrm{d}t}\int_{\Omega^h(t)} C\hat{C}\,\mathrm{d}\Omega - \int_{\Omega^h(t)} C\left(\mathbf{u}\cdot\boldsymbol{\nabla}\hat{C} + \tilde{w}\frac{\partial\hat{C}}{\partial z}\right)\mathrm{d}\Omega + \int_{\Gamma_s^h} C\hat{C}\left(\mathbf{u}\cdot\mathbf{n} + \tilde{w}n_z\right)\mathrm{d}\tau \\ &+ \int_{\Omega^h(t)} \kappa\left(\boldsymbol{\nabla}\hat{C}\cdot\boldsymbol{\nabla}C + \frac{\partial\hat{C}}{\partial z}\frac{\partial C}{\partial z}\right)\mathrm{d}\Omega = 0 \quad \forall\,\hat{C}\in\mathcal{G}.\end{aligned} \tag{22}$$

3.3 Finite element discretization

We now seek approximations $\eta^h \simeq \eta$, $w^h \simeq w$ and $C^h \simeq C$ in finite-dimensional subsets of $\mathcal{H}$, $\mathcal{W}$ and $\mathcal{G}$, respectively. Each of those subsets, marked by a superscript h, is spanned by a finite number of polynomial basis functions. The basis functions will be noted ψ with a superscript indicating the variable to which it is associated. The finite element approximations are

$$\begin{aligned}
\eta \quad &\simeq \eta^h = \sum_{j=1}^{N_\eta} H_j(t)\psi_j^\eta(x,y) && \in \mathcal{H}^h = \mathrm{span}\left\{\psi_1^\eta,\ \psi_2^\eta,\ \ldots,\ \psi_{N_\eta}^\eta\right\} && \subset \mathcal{H},\\
w \quad &\simeq w^h = \sum_{j=1}^{N_w} W_j(t)\psi_j^w(x,y,z) && \in \mathcal{W}^h = \mathrm{span}\left\{\psi_1^w,\ \psi_2^w,\ \ldots,\ \psi_{N_w}^w\right\} && \subset \mathcal{W},\\
C \quad &\simeq C^h = \sum_{j=1}^{N_C} C_j(t)\psi_j^C(x,y,z) && \in \mathcal{G}^h = \mathrm{span}\left\{\psi_1^C,\ \psi_2^C,\ \ldots,\ \psi_{N_C}^C\right\} && \subset \mathcal{G}.
\end{aligned} \tag{23}$$

Note that, strictly speaking, the three-dimensional basis functions depend on time due to the mesh motions. This, however, only has an implication on the tracer equation where a time derivative appears. We now opt for the Galerkin method, which is equivalent to the following procedure. Consider each variational statement, Eqs (15), (17) and (22), in which the sought variable (η, w and C) is substituted for its approximation (η^h, w^h and C^h, respectively) and hold it true when the test function is substituted for any of the basis functions spanning the corresponding subset to which the test function belongs. We also assume that we possess an approximation $\mathbf{u}^h$ of the horizontal velocity field, the obtainment of which is beyond the scope of this paper (see White et al. (submitted) instead).

The discrete variational statement for the elevation, Eq. (15), now consists in finding $\eta^h \in \mathcal{H}^h$ such that

$$\int_{\mathcal{T}^h} \frac{\partial\eta^h}{\partial t}\psi_i^\eta\,\mathrm{d}\tau - \int_{\Omega^h} \mathbf{u}^h\cdot\boldsymbol{\nabla}\psi_i^\eta\,\mathrm{d}\Omega = 0 \quad \forall\, i = 1,\ 2,\ \ldots,\ N_\eta. \tag{24}$$

For the continuity equation, the discrete variational statement consists in finding $w^h \in \mathcal{W}^h$ such that

$$\begin{aligned}&-\int_{\Omega^h}\left[\mathbf{u}^h\cdot\boldsymbol{\nabla}\psi_i^w + w^h\frac{\partial\psi_i^w}{\partial z}\right]\mathrm{d}\Omega \\ &+\int_{\Gamma_s^h}\psi_i^w\left(\mathbf{u}^h\cdot\mathbf{n} + w^h n_z\right)\mathrm{d}\tau = 0 \quad \forall\, i = 1,\ 2,\ \ldots,\ N_w.\end{aligned} \tag{25}$$

Finally, the discrete variational statement for the tracer equation consists in finding $C^h \in \mathcal{G}^h$ such that

$$\begin{aligned}&\frac{\mathrm{d}}{\mathrm{d}t}\int_{\Omega^h(t)} C^h\psi_i^C\,\mathrm{d}\Omega - \int_{\Omega^h(t)} C^h\left(\mathbf{u}^h\cdot\boldsymbol{\nabla}\psi_i^C + \tilde{w}^h\frac{\partial\psi_i^C}{\partial z}\right)\mathrm{d}\Omega \\ &+\int_{\Gamma_s^h} C^h\psi_i^C\left(\mathbf{u}^h\cdot\mathbf{n} + \tilde{w}^h n_z\right)\mathrm{d}\tau + \int_{\Omega^h(t)}\kappa\left(\boldsymbol{\nabla}\psi_i^C\cdot\boldsymbol{\nabla}C^h + \frac{\partial\psi_i^C}{\partial z}\frac{\partial C^h}{\partial z}\right)\mathrm{d}\Omega = 0 \\ &\forall\, i = 1,\ 2,\ \ldots,\ N_C.\end{aligned} \tag{26}$$

3.4 Discrete conservation laws

Starting from the discrete variational statements (24), (25) and (26), we now investigate under which conditions global volume and tracer conservation as well as consistency (i.e., compatibility) are achieved in the discrete sense.

3.4.1 Volume conservation

Since the variational formulation (24) must be valid for any ψ_i^η, it must hold true for $\psi_i^\eta = 1$ as well (which belongs to $\mathcal{H}^h$). Setting $\psi_i^\eta = 1$ in Eq. (24) and using the fact that $\mathcal{T}^h$ is time-independent gives rise to

$$\frac{\mathrm{d}}{\mathrm{d}t}\int_{\mathcal{T}^h} \eta^h \, \mathrm{d}\tau = 0, \tag{27}$$

which is the discrete statement of volume conservation.

3.4.2 Global tracer conservation

The property of global tracer conservation is investigated by setting $\psi_i^C = 1$ in the discrete variational statement for the tracer equation, Eq. (26). We then obtain

$$\frac{\mathrm{d}}{\mathrm{d}t}\int_{\Omega^h(t)} C^h \, \mathrm{d}\Omega + \int_{\Gamma_s^h} C^h \left[\mathbf{u}^h \cdot \mathbf{n} + (w^h - w_m^h) n_z\right] \mathrm{d}\tau = 0, \tag{28}$$

where we used $\tilde{w}^h = w^h - w_m^h$. In view of Eq. (28), providing that the integral over the free surface Γ_s^h is discarded, the tracer is globally conserved, namely

$$\frac{\mathrm{d}}{\mathrm{d}t}\int_{\Omega^h(t)} C^h \, \mathrm{d}\Omega = 0. \tag{29}$$

However, discarding this integral consistently, that is while preserving the discrete compatibility between the elevation, continuity and tracer equations, brings about additional constraints as we will now see.

3.4.3 Consistency

According to the definition presented earlier, consistency is equivalent to requiring that a constant concentration be solution to Eq. (26). Setting $C^h = C_0 \neq 0$ in Eq. (26), factoring out C_0 and separating out the terms depending on the mesh velocity (and integrating them by parts) from those that do not, we end up having to satisfy the following equation

$$\begin{aligned} &\underbrace{\frac{\mathrm{d}}{\mathrm{d}t}\int_{\Omega^h(t)} \psi_i^C \, \mathrm{d}\Omega}_{A_1} - \underbrace{\int_{\Omega^h(t)} \psi_i^C \frac{\partial w_m^h}{\partial z} \, \mathrm{d}\Omega}_{A_2} - \underbrace{\int_{\Omega^h(t)} \left(\mathbf{u}^h \cdot \boldsymbol{\nabla}\psi_i^C + w^h \frac{\partial \psi_i^C}{\partial z}\right) \mathrm{d}\Omega}_{B_1} \\ &+ \underbrace{\int_{\Gamma_s^h} \psi_i^C \left(\mathbf{u}^h \cdot \mathbf{n} + w^h n_z\right) \mathrm{d}\tau}_{B_2} = 0 \quad \forall\, i = 1,\ 2,\ \ldots,\ N_C. \end{aligned} \tag{30}$$

The A_2-labeled term is the result of integrating by parts all terms involving the mesh velocity. The set of B-labeled terms in the above expression and the discrete variational statement for the continuity equation, Eq. (25), are identical under the following two conditions:

1. the subsets $\mathcal{W}^h$ and $\mathcal{G}^h$ are the same (in which case $\psi_i^w = \psi_i^C \ \forall i = 1,\ 2,\ \ldots\ N^w = N^C$),
2. the B-labeled terms and Eq. (25) are computed on the same mesh $\Omega^h(t)$.

These two conditions may be summarized by simply demanding that Eq. (25) and the advection terms in Eq. (30) be discretely compatible, a condition that we will call discrete compatibility between the continuity and tracer equations. Concretely, this entails that the same elements must be used to compute w^h and C^h. Note that this condition is conceptually the same as that derived when using finite differences (Griffies et al., 2001). Now, the fulfillment of this condition does not necessarily ensure that Eq. (30) is satisfied. The following relation between the A-labeled terms of Eq. (30) must also hold true :

$$\frac{\mathrm{d}}{\mathrm{d}t}\int_{\Omega^h(t)} \psi_i^C \, \mathrm{d}\Omega = \int_{\Omega^h(t)} \psi_i^C \frac{\partial w_m^h}{\partial z} \, \mathrm{d}\Omega. \tag{31}$$

When using a discontinuous representation, the above expression must be true for each element $\Omega_e(t)$ individually when $\psi_i^C = 1$, which is a stricter condition. When discretized in time and when $\psi_i^C = 1$, Eq. (31) becomes

$$\mathrm{VOL}\left(\Omega_e^{n+1}\right) - \mathrm{VOL}\left(\Omega_e^n\right) = \int_{t^n}^{t^{n+1}} \left(\int_{\Omega_e(t)} \frac{\partial w_m^h}{\partial z} \, \mathrm{d}\Omega\right) \mathrm{d}t, \tag{32}$$

where the time step shall be defined as $\Delta t = t^{n+1} - t^n$. Eq. (32) is known as the Discrete Geometric Conservation Law (DGCL) (Farhat et al., 2001; Donea et al., 2004; Formaggia and Nobile, 2004) and states that the variation in volume of a given element over Δt must be equal to the volume swept by the element boundaries (with velocity w_m) during that time interval. Note that if the volume is computed exactly, then the time integration in the right-hand side of (32) must be exact. Depending upon the hypotheses made regarding the time dependence of w_m^h, a proper quadrature rule must then be used. Hence, to ensure consistency, the following two conditions at least must be fulfilled:

1. the continuity and tracer equations must be discretely compatible (i.e., the way we compute the vertical velocity must be discretely compatible with the way we compute the advection terms in the tracer equation),

2. the mesh update procedure must comply with the DGCL (see Eq. 32).

It should be emphasized that these conditions involve the continuity and tracer equations as well as the mesh update procedure. So far, nothing has been said regarding the free-surface elevation equation.

Conserving the tracer globally while preserving consistency between the continuity and tracer equations requires that the surface integral on Γ_s^h automatically vanish when $C^h = 1$ in Eq. (28). This will happen only if the computation of the vertical velocity guarantees it. We now verify that this is the case. Let us return to the continuity equation and focus on the discrete variational statement, Eq. (25). Since the mesh is made up of prisms with vertical faces, we can readily add up the components of Eq. (25) written for those ψ_i^w sharing the same two-dimensional support. We note I the set of indices i corresponding to the basis functions ψ_i^w aligned on the same vertical. By definition, all these basis functions satisfy the following two properties:

$$\sum_{i\in I} \psi_i^w(x,y,z) = \psi_I^{w,2D}(x,y),$$
$$\sum_{i\in I} \frac{\partial \psi_i^w}{\partial z}(x,y,z) = 0,$$

where $\psi_I^{w,2D}$ is simply the projection of ψ_i^w ($i \in I$) onto the plane (x,y). This projection is identified by I. The first summation translates the fact that the vertical dependences of all basis functions cancel out. Now, adding up the components of (25) in the vertical gives rise to

$$-\int_{\Omega^h} \mathbf{u}^h \cdot \boldsymbol{\nabla} \psi_I^{w,2D} \mathrm{d}\Omega + \int_{\Gamma_s^h} \psi_I^{w,2D} \left(\mathbf{u}^h \cdot \mathbf{n} + w^h n_z\right) \mathrm{d}\tau = 0. \tag{33}$$

The similarities between the above expression and the discrete variational statement for the elevation, Eq. (24), are clear. By choosing the basis functions for the vertical velocity such that $\psi_I^{w,2D} = \psi_I^\eta$, where ψ_I^η is the two-dimensional elevation basis function, the second term in the discrete elevation equation (Eq. 24) is identical to the first term in Eq. (33). This leaves us with the following equality:

$$\int_{\Gamma_s^h} \psi_I^{w,2D} \left(\mathbf{u}^h \cdot \mathbf{n} + w^h n_z\right) \mathrm{d}\tau = \int_{\mathcal{T}^h} \psi_I^\eta \frac{\partial \eta^h}{\partial t} \, \mathrm{d}\tau = \int_{\Gamma_s^h} \psi_I^\eta \frac{\partial \eta^h}{\partial t} n_z \, \mathrm{d}\tau$$

where n_z is the Jacobian of the transformation of coordinates from $\mathcal{T}^h$ to Γ_s^h. The last expression thus becomes

$$\int_{\Gamma_s^h} \psi_i^w \left\{ \mathbf{u}^h \cdot \mathbf{n} + \left(w^h - \frac{\partial \eta^h}{\partial t} \right) n_z \right\} \mathrm{d}\tau = 0, \tag{34}$$

where we used the fact that ψ_i^w reduces to its two-dimensional structure on Γ_s^h. Eq. (34) is the discrete counterpart of the kinematic boundary condition on the vertical velocity, given by Eq. (7). Most importantly, this result demonstrates that global conservation can be achieved without breaking down consistency. When setting $C^h = 1$ in Eq. (26), the surface integral on Γ_s^h vanishes if the mesh velocity at the sea surface is $w_m^h = \frac{\partial \eta^h}{\partial t}$ and the same interpolation is used in the horizontal for the elevation and the vertical velocity. Under these two conditions, the surface integral can be discarded consistently in Eq. (28).

The discrete surface kinematic boundary condition is retrieved by adding up the discrete components of the continuity equation in the vertical. This is a consequence of the elevation and continuity equations being discretely compatible. And they should be since they express the same principle of volume conservation. It then turns out that the surface kinematic boundary condition is redundant, complying with the first-order nature of the continuity equation. In the appendix, we show that integrating

the continuity equation downward (with the imposition of the surface boundary condition) allows for automatically retrieving the seabed boundary condition, provided of course that the continuity and elevation equations be discretely compatible. Both directions of integration yield equivalent results (the correct boundary condition is retrieved) and the tracer conservation does not depend on it (the tracer is consistently conserved in both cases). It is easy to conjure up a way of breaking down consistency while preserving global conservation. By enforcing the surface tracer flux to vanish, global conservation is ensured. However, if there is no compatibility between the elevation and the continuity equations, this surface integral does not naturally vanish and consistency breaks down. Now, an opposite scenario can be imagined. Consistency is easily achieved by ensuring that the tracer and continuity equations are discretely compatible. Nevertheless, if the surface integral does not vanish and is computed (to ensure consistency), global conservation will break down for a tracer distribution different than a constant value throughout the domain.

The key results regarding conservation are summarized below. In the absence of source terms and diffusive boundary fluxes, sufficient conditions to consistently achieve global tracer conservation are the following.

1. The continuity and tracer equations are discretely compatible, which comes down to having the discrete advection terms in the tracer equation reduce to the discrete continuity equation when $C^h = 1$ (see Eq. 30).

2. The DGCL is satisfied elementwise (see Eq. 32).

3. The elevation and continuity equations are discretely compatible. This condition entails that the discrete surface kinematic boundary condition is retrieved when adding up all components of the discrete continuity equation in the vertical (see Eq. 34).

4. The mesh velocity at the surface Γ_s^h is oriented in the z-direction and has a magnitude $w_m^h = \frac{\partial \eta^h}{\partial t}$. Note that, in the interior, the mesh motion is not constrained unless element shape regularity requires it.

3.5 Which elements should we use ?

The above conditions restrict the choice of finite element subsets and, thereby, the choice of elements that can be used. These restrictions lead to the following guidelines. (i) The same element must be used for the vertical velocity and the tracer. (ii) The nodes location in the horizontal must be the same for the elevation and the vertical velocity. (iii) The two previous statements also imply that the nodes location in the horizontal must be the same for the elevation, the vertical velocity and the tracer. (iv) In the vertical, the nodes location for the vertical velocity and the tracer is unconstrained, yet it must be identical for both variables.

In addition to these considerations, the mixed formulation used for the horizontal velocity and the elevation must be numerically stable. The mixed formulation should be devoid of spurious elevation and velocity modes. In the presence of spurious elevation modes, a stabilized formulation can usually filter out the modes. However, this requires to add a term to the discrete elevation equation, with the consequence of breaking down the discrete compatibility between the elevation and continuity equations. Velocity modes are less problematic insofar as a small amount of momentum diffusion is usually sufficient to filter them out. Based on the most recent studies, the two mixed formulations that turn out to be the most effective for hydrostatic marine modeling based on the primitive equations are the $P_1^{NC} - P1$ and the RT_0 pairs (Hanert and Deleersnijder, 2003; Le Roux, 2005; Le Roux et al., 2005, in press). The first pair was originally used by Hua and Thomasset (1984) for shallow-water flows and consists of a linear non-conforming interpolation for both components of the velocity and a linear interpolation for the elevation. It does not support any spurious oscillations. This pair has been used by Hanert et al. (2005) and White et al. (2006a) in two dimensions and by White and Deleersnijder (in press) in three dimensions. The second pair is called low-order Raviart-Thomas element. The normal velocity components are located at the middle of each side of the triangular element and the elevation is constant on each element. Shallow-water models using this formulation are described by Miglio et al. (1998) and Walters (2005).

Using the $P_1^{NC} - P_1$ pair requires to opt for a P_1 representation in the horizontal for the tracer and the vertical velocity (in order to consistently ensure global conservation). To fulfill the same property with the RT_0 element, the vertical velocity and the tracer must be constant in the horizontal on each element. In both cases, there is no constraint for the vertical interpolation: it could be of high order and discontinuous. Both schemes have advantages and disadvantages. A linear continuous representation

for the tracers is not optimal for advection-dominated flows. Stabilization could be necessary (without impact on conservation). The finite volume scheme pertaining to the RT_0 element is certainly more stable but might be overdiffusive. Regarding the elevation, P_1 is more accurate than P_0 with the latter leading to twice as many degrees of freedom. Moreover, a P_1 interpolation for the elevation leads to a piecewise linear (and continuous) representation of the moving mesh. Finally, when using the $P_1^{NC} - P_1$ pair, to be computationally competitive, the matrices of the systems to compute the vertical velocity and the tracer must be rendered at least banded diagonal through mass lumping

3.6 The issue of time stepping

In light of the developments carried out above, time discretization does not appear to be an issue. However, there is more into conservation than the proper choice of elements for spatial discretization. To ensure a discrete compatibility between the free-surface elevation and the continuity equations – and thus, to consistently ensure global tracer conservation –, the following property must be satisfied. The horizontal transport whose divergence is responsible for the change in the free-surface elevation must be equal to the horizontal transport associated with the horizontal velocity used to compute the vertical velocity. These transports are not necessarily equal and when that occurs, the three-dimensional horizontal velocity must be corrected so that its transport is equal to that used to compute the free-surface elevation. The main cause for this discrepancy originates from the choice of time stepping. If a semi-implicit scheme is considered for the inertia-gravity wave terms (with or without mode splitting), the horizontal transport causing the elevation change from time steps n to $n+1$ is the mean transport computed from those at time steps n and $n+1$. The three-dimensional horizontal velocity must then be corrected accordingly. Following this procedure, linearizing the elevation equation poses no problem as far as conservation is concerned. However, it has been suggested in the past that this approach prevents tracers to be conserved because the domain does not move (Roullet and Madec, 2000). In fact, when we opt for such a linearized elevation equation, we may still alter the domain geometry according to the free-surface motions. To preserve the property of consistent conservation (i.e., discrete compatibility between the elevation and continuity equations), the three-dimensional horizontal velocity must be corrected to yield a transport in the deformed domain that is equal to the transport (in the undeformed domain) used in the linearized elevation equation.

4 Illustrative experiments

A few numerical experiments using SLIM[1] are now presented. In its current configuration, the model conserves the volume and any tracer globally up to machine precision in a consistent way. The Goldsbrough-Stommel circulation, induced by freshwater fluxes, is addressed as a first illustrative experiment. We then investigate the implications of a consistency breakdown.

4.1 Model description

The model SLIM is described in detail by White et al. (submitted). We now briefly recall its most important features. The dynamics is split into a two-dimensional depth-averaged system for the evolution of the fast-propagating surface waves and a three-dimensional system for the vertical structure of the velocity. The same time step is used for both systems and all terms governing the propagation of inertia-gravity waves are semi-implicit in time. The elements used to interpolate the elevation and the velocity are depicted in Figure (3). The mixed formulation $P_1^{NC} - P_1$ is used for the horizontal velocity and the elevation, respectively. In order to be consistent with this choice, a linear continuous interpolation is used for the vertical velocity and all tracers. All velocity components and tracers are interpolated with linear discontinuous basis functions in the vertical.

4.2 The Goldsbrough-Stommel circulation

The Goldsbrough-Stommel circulation discussed by Huang and Schmitt (1993) and Huang (1993) arises from freshwater forcing and is absent in rigid-lid models. A decent rendition of the barotropic flow induced by freshwater forcing alone in the North Atlantic basin is obtained by assuming the following simple linear profile for the freshwater flux q_w (see Eq. 3):

$$q_w = -q_{w0}\left[1 - 2\frac{(y - y_s)}{(y_n - y_s)}\right],$$

[1] Second-generation Louvain-la-Neuve Ice-ocean Model (`http://www.climate.be/SLIM`).

where y is the meridional coordinate and y_s and y_n are the southern and northern coordinates of the basin, respectively. The freshwater flux magnitude is given by q_{w0}. This linear profile is an idealization of observations (Huang and Schmitt, 1993) and integrates to zero over the domain so that the total volume remains constant. We aim at comparing our results with that previously presented by Huang (1993) and Griffies et al. (2001). In both studies, the models were set up in spherical coordinates on a basin confined between the equator and 60°N and extending 60° zonally. Our model was run on a square basin of size 5000 km and constant depth of 4000 m. Following Huang (1993), the coefficients of horizontal and vertical viscosity are 5×10^4 m^2 s^{-1} and 10^{-4} m^2 s^{-1}, respectively. The equations are solved in Cartesian coordinates on a β-plane centered at 30°N. Neglecting the earth curvature on these scales is questionable. However, the objective of this experiment is twofold. First, we want to assess the model's ability at naturally handling freshwater fluxes as a simple forcing term in the elevation equation. Second, we want to evaluate the model's response in terms of surface salinity due to a local volume variation.

As shown in Figure (4), our results compare well to that of Huang (1993) and Griffies et al. (2001). Three meshes were used, each one with increased resolution along the western boundary (see caption of Figure (4) for details on mesh resolution). All meshes comprise four equally-spaced layers of prisms. Since the resulting flow is barotropic, the number of layers has no effect on the numerical result. Both the anticyclonic subpolar and cyclonic subtropical gyres are well represented. The separation between both gyres lies at three fifths of the domain extent, in good agreement with results by Huang (1993) and Griffies et al. (2001). The barotropic volume transport is less than one Sv (1 Sv = 10^6 m^3 s^{-1}), which is only a few percent of the wind-driven and thermally-driven transport. However, as hinted by Figure (5) representing the surface salinity after three years, this tiny freshwater flux can potentially drive a strong three-dimensional baroclinic circulation. The freshwater input and output locally causes an increase and decrease, respectively, in the ocean volume. This, in turn, locally dilutes and concentrates the salt and a horizontal salinity gradient builds up at the surface. This dilution/concentration effect is only due to a variation in the volume of the ocean. The tracer flux at the sea surface is zero and the total salt contents is conserved. In our experiment, salinity acts as a passive tracer: it does not feed back the flow. The coefficients of horizontal and vertical eddy diffusivity are 10^3 m^2 s^{-1} and 10^{-4} m^2 s^{-1}, respectively. For thorough studies of the freshwater-driven baroclinic circulation, see Huang (1993), Huang and Chou (1994) and Rahmstorf (1996).

4.3 When consistency breaks down

The results shown thus far have been obtained by solving the consistent discrete equations, with nodes location depicted in Figure (3). We now study cases in which the elements for the vertical velocity w and the tracer C are different and whereby consistency breaks down. In all experiments described in this section, the elements used for the vertical velocity and the elevation are those depicted in Figure (3). We use different elements for the tracer.

In Figure (6), three situations are compared. The model is run on a 10 km wide and 20 m deep square basin. The initial elevation field is a 2 m high Gaussian that we let freely evolve as a gravity wave over 1000 time steps of 72 s. The initial tracer concentration is 1 and should remain equal to 1 at all time (there is no boundary flux and no source term). The surface integral in Eq. (28) is discarded to ensure global tracer conservation in all situations. All simulations are carried out on the three-dimensional mesh shown in Figure (7), comprising five equally-spaced layers of prisms. In the first experiment, we use the same element for w and C. All consistency conditions are fulfilled and this is verified numerically. The deviations in the surface tracer concentration are zero (up to machine precision). In the second and third experiments, the element for C is linear non-conforming and remains linear discontinuous in the vertical. The non-conforming representation in the horizontal is particularly well suited for advection-dominated flows (Hanert et al., 2004), which is the reason behind this choice. When solving the advection equation for the tracer (i.e., without diffusion), the deviations at the surface reach very high values that are unbounded numerically and grow unstably (see second experiment in Figure 6). In the third experiment, horizontal diffusion is added ($\kappa = 10$ m^2 s^{-1}), which drastically reduces the deviations at the surface. Since the largest deviations are typically confined within the upper layers of the domain, they could be alleviated by choosing an appropriate diffusion coefficient.

In Figure (8), similar experiments (without diffusion) are carried out on domains with spatial scales ranging from 10 km (shelf scale) to 1000 km (basin scale) with increasing depths, yet setting off all experiments with the same 2 m high Gaussian (the parameters of the simulation are recalled in the figure). These runs were carried out in an attempt at getting some insights on the effect of a consistency breakdown on flows spanning a wide range of spatial scales. As we have already seen, the consequences are quite dramatic for the smallest domain (which is the same experiment as that corresponding to the

middle panel of Figure 6). For larger domains, the surface deviations remain below one percent. Since the deviations of the tracer are caused by the inconsistent treatment of the the advection terms, it might be expected that as soon as those terms grow larger in magnitude, those deviations will increase. For the small domain, the flow speed is on the order of 0.3 m s^{-1} while it decreases to roughly 0.08 m s^{-1} and 0.01 m s^{-1} for the intermediate and larger domains, respectively. If we set the order of magnitude of the advection terms to 1 for the small domain, advection has a relative magnitude of 7×10^{-3} and 10^{-5} for the intermediate and larger domains, respectively. This sheds light on the results obtained in Figure (8).

Modeling flows in coastal and shelf regions where advection is dominant definitely requires to use a consistent spatial scheme. Failing to do so may not only generate spurious currents but also numerical instabilities. Finally, one might argue that, for the large-scale ocean circulation, inconsistency is not problematic and could be easily tackled by adding some horizontal diffusion. We do contend, however, that even in those cases where advection is weak, conservation and consistency must be achieved to machine precision if the model is to be trusted at all for climate simulations, especially for those models coupled with biogeochemical cycles (Gnanadesikan, 1999; Griffies et al., 2005). If these properties are not strictly satisfied, the physical integrity of the numerical solution will eventually degrade down to an unpredictable state.

5 Conclusions

In this paper, we have summarized sufficient conditions in terms of the finite element spatial discretization of a three-dimensional hydrostatic marine model to consistently conserve any tracer globally. A consistent (or discretely compatible) spatial scheme is defined as one that maintains the uniform tracer concentration set initially (when there is no boundary flux and no source term). The following conditions must be fulfilled to satisfy those properties. (i) The same interpolation must be used in the horizontal for the elevation, the vertical velocity and the tracer. (ii) The same interpolation in the vertical must be used for the vertical velocity and the tracer. (iii) The mesh update procedure must satisfy the Discrete Geometric Conservation Law. (iv) The mesh velocity at the surface must be equal to $\frac{\partial \eta}{\partial t}$. These considerations must be complemented by the necessity of choosing a stable finite-element pair for the primitive shallow-water equations.

Several numerical experiments were carried out to show the model's ability at responding to freshwater forcing. In particular, we showed how the variation in the domain volume naturally leads to dilution and concentration of salt. We finally performed a series of experiments in which consistency between the vertical velocity and the concentration was deliberately broken down. If consistency must be ensured for advection-dominated flows typical in coastal and shelf regions, it was shown that using an inconsistent scheme for larger-scale application could be a viable alternative. However, even for those problems, diffusion-based remedies could not work out in regions where advection becomes more important (e.g., boundary currents regions).

Acknowledgments

Laurent White and Eric Deleersnijder are a Research fellow and a Research associate, respectively, with the Belgian National Fund for Scientific Research (FNRS). The present study was carried out within the scope of the project "A second-generation model of the ocean system", which is funded by the *Communauté Française de Belgique*, as *Actions de Recherche Concertées*, under contract ARC 04/09-316. This work is a contribution to the construction of SLIM, the Second-generation Louvain-la-Neuve Ice-ocean Model (http://www.climate.be/SLIM).

APPENDIX

Downward integration of the continuity equation

In the body of the article, the continuity equation is integrated upwards after imposing the kinematic boundary condition at the seabed. By doing so, the discrete surface kinematic boundary condition is automatically retrieved. Herein, we show that an equivalent result is obtained by integrating the continuity equation downwards after imposing the kinematic boundary condition at the surface. Let us

consider the discrete variational statement for the continuity equation, inferred from Eq. (25), in which boundary conditions are yet to be prescribed. We have

$$-\int_{\Omega^h}\left[\mathbf{u}^h\cdot\boldsymbol{\nabla}\psi_i^w+w^h\frac{\partial\psi_i^w}{\partial z}\right]\mathrm{d}\Omega+\int_{\Gamma_b^h}\psi_i^w\left(\mathbf{u}^h\cdot\mathbf{n}+w^h n_z\right)\mathrm{d}\tau$$
$$+\int_{\Gamma_s^h}\psi_i^w\left(\mathbf{u}^h\cdot\mathbf{n}+w^h n_z\right)\mathrm{d}\tau=0\quad\forall\, i=1,\ 2,\ \ldots,\ N_w.$$

Imposing the discrete counterpart of the surface kinematic boundary condition (7) gives rise to

$$-\int_{\Omega^h}\left[\mathbf{u}^h\cdot\boldsymbol{\nabla}\psi_i^w+w^h\frac{\partial\psi_i^w}{\partial z}\right]\mathrm{d}\Omega+\int_{\Gamma_b^h}\psi_i^w\left(\mathbf{u}^h\cdot\mathbf{n}+w^h n_z\right)\mathrm{d}\tau$$
$$+\int_{\Gamma_s^h}\psi_i^w\frac{\partial\eta^h}{\partial t}n_z\mathrm{d}\tau=0\quad\forall\, i=1,\ 2,\ \ldots,\ N_w.$$

We may now add up all components of the above expression pertaining to those test functions ψ_i^w sharing the same two-dimensional support (the indices belong to the set I). This yields the following expression, written for the two-dimensional projection of ψ_i^w ($i\in I$), noted $\psi_I^{w,2D}$:

$$-\int_{\Omega^h}\mathbf{u}^h\cdot\boldsymbol{\nabla}\psi_I^{w,2D}\mathrm{d}\Omega+\int_{\Gamma_b^h}\psi_I^{w,2D}\left(\mathbf{u}^h\cdot\mathbf{n}+w^h n_z\right)\mathrm{d}\tau+\int_{\Gamma_s^h}\psi_I^{w,2D}\frac{\partial\eta^h}{\partial t}n_z\mathrm{d}\tau=0.$$

If we choose the basis functions for the vertical velocity such that $\psi_I^{w,2D}=\phi_i$, where ϕ_i is the two-dimensional elevation basis function associated with the same nodal position in the (x,y)-plane, the first and third terms of the above equation are identically equal to the discrete elevation equation, Eq. (24), which leaves us with

$$\int_{\Gamma_b^h}\psi_I^{w,2D}\left(\mathbf{u}^h\cdot\mathbf{n}+w^h n_z\right)\mathrm{d}\tau=0,$$

namely the discrete counterpart of the kinematic boundary condition at the seabed, Eq. (6).

References

Aizinger, V. and C. Dawson, 2002: A discontinuous Galerkin method for two-dimensional flowand transport in shallow water. *Adv. Water Resour.*, **25**, 67–84.

Berger, R. C. and S. E. Howington, 2002: Discrete fluxes and mass balance in finite elements. **128**, 87–92.

Bernard, P.-E., N. Chevaugeon, VincentLegat, E. Deleersnijder, and J.-F. Remacle, accepted: High-order h-adaptive discontinuous Galerkin methodsfor ocean modeling. *Ocean Dynamics*.

Campin, J.-M., A. Adcroft, and C. H. andJohn Marshall, 2004: Conservation of properties in a free-surface model. *Ocean Model.*, **6**, 221–244.

Casulli, V. and R. A. Walters, 2000: An unstructured grid, three-dimensional model based on theshallow-water equations. *Int. J. Numer. Methods Fluids*, **32**, 331–346.

Cushman-Roisin, B. and C. E. Naimie, 2002: A 3D finite-element model of the Adriatic tides. *J. Mar. Syst.*, **37**, 279–297.

Danilov, S., G. Kivman, and J. Schröter, 2004: A finite-element ocean model: principles and evaluation. *Ocean Model.*, **6**, 125–150.

— 2005: Evaluation of an eddy-permitting finite-element ocean model in the North Atlantic. *Ocean Model.*, **10**, 35–49.

Dawson, C., J. J. Westerink, J. C. Feyen, and D. Pothina, 2006: Continuous, discontinuous and coupled discontinuous-continuous Galerkin finite element methods for the shallow water equations. *Int. J. Numer. Methods Fluids*, **52**, 63–88.

Deleersnijder, E., 1993: Numerical mass conservation in a free-surface sigmacoordinate marine model with mode splitting. *J. Mar. Syst.*, **4**, 365–370.

Deleersnijder, E. and J.-M. Campin, 1995: On the computation of the barotropic mode of a free-surfaceworld ocean model. *Ann. Geophys.*, **13**, 675–688.

Donea, J., A. Huerta, J.-P. Ponthot, and A.Rodríguez-Ferran, 2004: Arbitrary Lagrangian-Eulerian methods. *Encyclopedia of Computational Mechanics*, E. Stein, R. de Borst, and T. J. R. Hughes, eds., John Wiley and Sons, chapter 14.

Farhat, C., P. Geuzaine, and C. Grandmont, 2001: The discrete geometric conservation law and the nonlinearstability of ALE schemes for the solution of flow problems onmoving grids. *J. Comput. Phys.*, **174**, 669–694.

Flaherty, J. E., L. Krivodonova, J.-F. Remacle, and M. S. Shephard, 2002: Aspects of discontinuous Galerkin methods for hyperbolic conservation laws. *Finite Elements in Analysis and Design*, **38**, 889–908.

Ford, R., C. C. Pain, M. D. Piggott, A. J. H.Goddard, C. R. E. de Oliveira, and A. P. Umpleby, 2004a: A non-hydrostatic finite element model forthree-dimensional stratified oceanic flows. Part I: modelformulation. *Mon. Weather Rev.*, **132**, 2816–2831.

— 2004b: A non-hydrostatic finite element model forthree-dimensional stratified oceanic flows. Part II: modelvalidation. *Mon. Weather Rev.*, **132**, 2832–2844.

Formaggia, L. and F. Nobile, 2004: Stability analysis of second-order time accurate schemesfor ALE-FEM. *Comput. Meth. Appl. Mech. Eng.*, **193**, 4097–4116.

Fortunato, A. B., A. M. Baptista, and R. A. Luettich, 1997: A three-dimensional model of tidal currents in the mouth of the Tagus estuary. *Cont. Shelf Res.*, **17**, 1689–1714.

Fringer, O. B., M. Gerritsen, and R. L. Street, 2006: An unstructured-grid, finite-volume, nonhydrostatic,parallel coastal ocean simulator. *Ocean Model.*, **14**, 139–173.

Gnanadesikan, A., 1999: Numerical issues for coupling biological models with ispycnal mixing schemes. *Ocean Model.*, **1**, 1–15.

Gorman, G. J., M. D. Piggott, C. C. Pain, C. R. E. Oliveira, A. P. Umpleby, and A. J. H. Goddard, 2006: Optimisation based bathymetry approximation throughconstrained unstructured mesh adaptivity. *Ocean Model.*, **12**, 436–452.

Greenberg, D. A., F. E. Werner, and D. R. Lynch, 1998: A diagnostic finite element ocean circulation model inspherical-polar coordinates. *J. Atmos. Ocean. Technol.*, **15**, 942–958.

Griffies, S. M., 2004: *Fundamentals of Ocean Climate Models*. Princeton University Press, Princeton (New Jersey), 496 pp.

Griffies, S. M., C. Böning, F. O. Bryan, E. P. Chassignet, R. Gerdes, H. Hasumi, A. Hirst, A.-M.Treguier, and D. Webb, 2000: Developments in ocean climate modelling. *Ocean Model.*, **2**, 123–192.

Griffies, S. M., A. Gnanadesikan, K. W. Dixon, J. P. Dunne, R. Gerdes, M. J. Harrison, A. Rosati, J. L. Russell, B. L. Samuels, M. J. Spelman, M. Winton, and R. Zhang, 2005: Formulation of an ocean model for global climate simulations. *Ocean Science*, **1**, 45–79.

Griffies, S. M., R. C. Pacanowski, M. Schmidt, and V.Balah, 2001: Tracer conservation with an explicit free surface methodfor z-coordinate ocean models. *Mon. Weather Rev.*, **129**, 1081–1098.

Ham, D. A., J. Pietrzak, and G. S. Stelling, 2005: A scalable unstructured grid 3-dimensional finite volumemodel for the shallow water equations. *Ocean Model.*, **10**, 153–169.

Hanert, E. and V. L. E. Deleersnijder, 2003: A comparison of three finite elements to solve the linear-shallow water equations. *Ocean Model.*, **5**, 17–35.

Hanert, E., D. Y. Le Roux, and V. L. E. Deleersnijder, 2004: Advection shemes for unstructured grid ocean modelling. *Ocean Model.*, **7**, 39–58.

Hanert, E., D. Y. Le Roux, V. Legat, and E. Deleersnijder, 2005: An efficient Eulerian finite element method for the shallow water equations. *Ocean Model.*, **10**, 115–136.

Hua, B.-L. and F. Thomasset, 1984: A noise-free finite element scheme for the two-layershallow water equations. *Tellus Ser. A*, **36**, 157–165.

Huang, R. X., 1993: Real freshwater flux as a natural boundary condition for the salinity balance and thermohaline circulation forced by evaporation and precipitation. *J. Phys. Oceanogr.*, **23**, 2428–2446.

Huang, R. X. and R. L. Chou, 1994: Parameter sensitivity study of the saline circulation. *Clim. Dyn.*, **9**, 391–409.

Huang, R. X. and R. W. Schmitt, 1993: The Goldsbrough-Stommel circulation of the World Ocean. *J. Phys. Oceanogr.*, **23**, 1277–1284.

Hughes, T. J. R., L. Engel, L. Mazzei, and M. G.Larson, 2000: The continuous Galerkin method is locally conservative. *J. Comput. Phys.*, **163**, 467–488.

Iskandarani, M., D. B. Haidvogel, and J. P. Boyd, 1995: A staggered spectral element model with application to theoceanic shallow water equations. *Int. J. Numer. Methods Fluids*, **20**, 393–414.

Iskandarani, M., D. B. Haidvogel, and J. C. Levin, 2003: A three-dimensional spectral element model for the solutionof the hydrostatic primitive equations. *J. Comput. Phys.*, **186**, 397–425.

Killworth, P. D., D. Stainforth, D. J. Webb, and S. M.Paterson, 1991: The development of a free-surface Bryan-Cox-Semtner oceanmodel. *J. Phys. Oceanogr.*, **21**, 1333–1348.

Kinnmark, I., 1986: *The Shallow Water Wave Equations: Formulation,Analysis and Applications*, volume 15 of *Lecture Notes in Engineering*. Springer-Verlag, 187 pp.

Kolar, R. L., J. J. Westerink, M. E. Cantekin, and C. Blain, 1994: Aspects of nonlinear simulations using shallow-water modelsbased on the wave continuity equation. *Comput. Fluids*, **23**, 523–538.

Kubatko, E. J., J. J. Westerink, and C. Dawson, 2006a: *hp* Discontinuous Galerkin methods for advectiondominated problems in shallow water flow. *Comput. Meth. Appl. Mech. Eng.*, **196**, 437–451.

— 2006b: An unstructured grid morphodynamic model with adiscontinuous Galerkin method for bed evolution. *Ocean Model.*, **15**, 71–89.

Labeur, R. J. and J. D. Pietrzak, 2005: A fully three dimensional unstructured grid non-hydrostaticfinite element coastal model. *Ocean Model.*, **10**, 51–67.

Le Roux, D. Y., 2001: A new triangular finite-element with optimum constraintratio for compressible fluids. *SIAM J. Sci. Comput.*, **23**, 66–80.

— 2005: Dispersion relation analysis of the $P_1^{NC} - P_1$finite-element pair in shallow-water models. *SIAM J. Sci. Comput.*, **27**, 394–414.

Le Roux, D. Y., V. Rostand, and B. Pouliot, in press: Analysis of numerically-induced oscillations in 2Dfinite-element shallow-water models. Part I: inertia-gravitywaves. *SIAM J. Sci. Comput.*, in press.

Le Roux, D. Y., A. Sène, V. Rostand, and E.Hanert, 2005: On some spurious mode issues in shallow-water models usinga linear algebra approach. *Ocean Model.*, **10**, 83–94.

Le Roux, D. Y., A. Staniforth, and C. A. Lin, 1998: Finite elements for shallow-water equation ocean models. *Mon. Weather Rev.*, **126**, 1931–1951.

Legrand, S., E. Deleersnijder, E. Delhez, and V.Legat, accepted: Unstructured, anisotropic mesh generation for theNorthwestern European continental shelf, the continental slopeand the neighboring ocean. *Cont. Shelf Res.*.

Legrand, S., E. Deleersnijder, E. Hanert, and V. L. E. Wolanski, 2006: High-resolution unstructured meshes for hydrodynamic modelsof the Great Barrier Reef, Australia. *Estuar. Coast. Shelf Sci.*, **68**, 36–46.

Legrand, S., V. Legat, and E. Deleersnijder, 2000: Delaunay mesh generation for unstructured-grid oceangeneral circulation model. *Ocean Model.*, **2**, 17–28.

Lynch, D. R. and W. R. Gray, 1979: A wave equation model for finite element tidal computations. *Comput. Fluids*, **7**, 207–228.

Lynch, D. R., J. T. C. Ip, and C. E. N. andF. E. Werner, 1996: Comprehensive coastal circulation model with application to the Gulf of Maine. *Cont. Shelf Res.*, **16**, 875–906.

Lynch, D. R. and C. E. Naimie, 1993: The M2 tide and its residuals on the outer banks of theGulf of Maine. *J. Phys. Oceanogr.*, **23**, 2222–2253.

Lynch, D. R. and F. E. Werner, 1987: Three-dimensional hydrodynamics on finite elements. Part I: linearized harmonic model. *Int. J. Numer. Methods Fluids*, **7**, 871–909.

— 1991: Three-dimensional hydrodynamics on finite elements. Part II: non-linear time-stepping model. *Int. J. Numer. Methods Fluids*, **12**, 507–533.

Massey, T. C. and C. A. Blain, 2006: In search of a consistent and conservative mass flux forthe GWCE. *Comput. Meth. Appl. Mech. Eng.*, **195**, 571–587.

Miglio, E., A. Quarteroni, and F. Saleri, 1998: Finite element approximation of quasi-3D shallow water equations. *Comput. Meth. Appl. Mech. Eng.*, **174**, 355–369.

Muccino, J. C., W. G. Gray, and M. G. G. Foreman, 1997: Calculation of vertical velocity in three-dimensional, shallow-water equation, finite element models. *Int. J. Numer. Methods Fluids*, **25**, 779–802.

Myers, P. G. and A. J. Weaver, 1995: A diagnostic barotropic finite-element ocean circulationmodel. *J. Atmos. Ocean. Technol.*, **12**, 511–526.

Nair, R. D., S. J. Thomas, and R. D. Loft, 2005: A discontinuous Galerkin global shallow water model. *Mon. Weather Rev.*, **133**, 876–888, doi:10.1175/MWR2903.1.

Nechaev, D., J. Schröter, and M. Yaremchuk, 2003: A diagnostic stabilized finite-element ocean circulationmodel. *Ocean Model.*, **5**, 37–63.

Pain, C. C., M. D. Piggott, A. J. H. Goddard, F.Fang, G. J. Gorman, D. P. Marshall, M. D. Eaton, P. Power, and C. R. E. de Oliveira, 2004: Three-dimensional unstructured mesh ocean modelling. *Ocean Model.*, **10**, 5–33.

Pietrzak, J., E. Deleersnijder, and J. Schröter, eds., 2005: *The Second International Workshop on Unstructured Mesh Numerical Modelling of Coastal, Shelf and Ocean Flows*, volume 10 of *Ocean Model.*. Elsevier, 252 pp.

Pietrzak, J., M. Iskandarani, J. Schröter, and F. Lyard, eds., 2006: *The Third International Workshop on Unstructured Mesh Numerical Modelling of Coastal, Shelf and Ocean Flows*, volume 15 of *Ocean Model.*. Elsevier, 138 pp.

Piggott, M. D., C. C. Pain, G. J. Gorman, P. W.Power, and A. J. H. Goddard, 2005: h, r, and hr adaptivity with applications in numericalocean modelling. *Ocean Model.*, **10**, 95–113.

Power, P. W., M. D. Piggott, F. Fang, G. J. G. C. C. Pain, D. P. Marshall, A. J. H. Goddard, and I. M.Navon, 2006: Adjoint goal-based error norms for adaptive mesh oceanmodelling. *Ocean Model.*, **15**, 3–38.

Rahmstorf, S., 1996: On the freshwater forcing and transport of the Atlantic thermohaline circulation. *Clim. Dyn.*, **12**, 799–811.

Roullet, G. and G. Madec, 2000: Salt conservation, free surface and varying levels: a newformulation for ocean general circulation models. *J. Geophys. Res.*, **105**, 23927–23942.

Schwanenberg, D. and M. Harms, 2004: Discontinuous Galerkin finite-element method fortranscritical two-dimensional shallow water flows. **130**, 412–421.

Schwanenberg, D., R. Kiem, and J. Kongeter, 2000: A discontinuous Galerkin method for the shallow-waterequations with source terms. *Discontinuous Galerkin Methods: Theory, Computationsand Applications*, B. Cockburn, G. E. Karniadaki, and C.-W. Chu, eds., Springer, Berlin, volume 11 of *Lecture Notes in Computational Science and Engineering*, 419–424.

Walters, R. A., 1992: A three-dimensional, finite element model for coastal andestuarine circulation. *Cont. Shelf Res.*, **12**, 83–102.

— 2005: Coastal ocean models: two useful finite element methods. *Cont. Shelf Res.*, **25**, 775–793.

— 2006: Design considerations for a finite element coastal oceanmodel. *Ocean Model.*, **15**, 90–100, doi:10.1016/j.ocemod.2005.11.002.

Walters, R. A. and F. E. Werner, 1989: A comparison of two finite element models of tidalhydrodynamics using the North Sea data set. *Adv. Water Resour.*, **12**, 184–193.

White, L., J.-M. Beckers, E. Deleersnijder, and V. Legat, 2006a: Comparison between free-surface and rigid-lid finite element models of barotropic instabilities. *Ocean Dynamics*, **56**, 86–103, doi:10.1007/s10236-006-0059-0.

White, L. and E. Deleersnijder, in press: Diagnoses of vertical transport in a three-dimensionalfinite-element model of the tidal circulation around an island. *Estuar. Coast. Shelf Sci.*, doi:10.1016/j.ecss.2006.07.014.

White, L., E. Deleersnijder, and V. Legat, submitted: A three-dimensional unstructured mesh finite element marinemodel, with application to the flow around a shallow-waterisland. *J. Geophys. Res.*.

White, L., V. Legat, E. Deleersnijder, and D. Le Roux, 2006b: A one-dimensional benchmark for the propagation of Poincaré waves. *Ocean Model.*, **15**, 101–123, doi:10.1016/j.ocemod.2005.11.001.

List of Figures

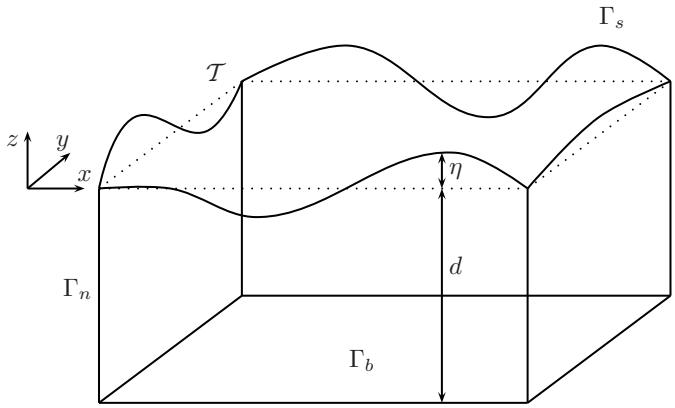

Figure 1: Notations used to describe the three-dimensional time-dependent domain Ω. The seabed and the free surface are denoted by Γ_b and Γ_s, respectively. The unperturbed plane defined by $z = 0$ is noted $\mathcal{T}$ and is represented by the dotted lines. The lateral boundary is noted Γ_n. At any location (x, y), the depth $d(x, y)$ and the elevation $\eta(x, y, t)$ are both defined with reference to $\mathcal{T}$. The displacement of the free surface is exaggerated.

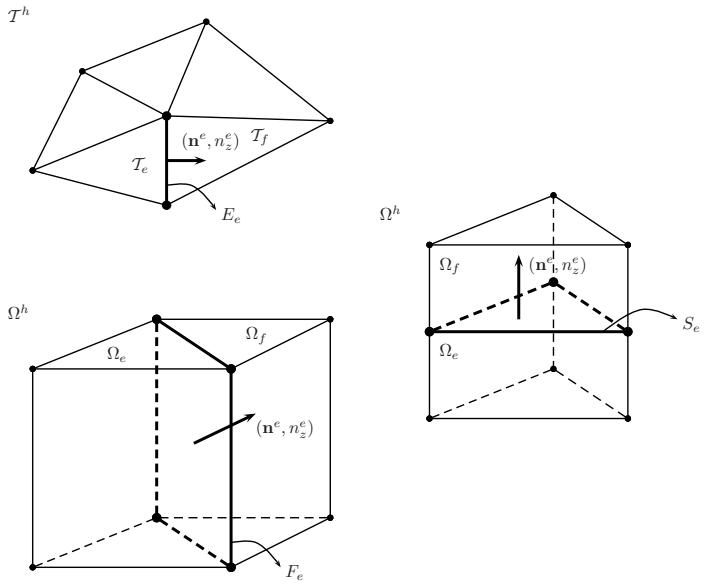

Figure 2: Main notations used to describe the mesh topology. In two dimensions, any interior edge E_e is shared by two triangles $\mathcal{T}_e$ and $\mathcal{T}_f$. In three dimensions, any interior vertical face F_e is common to adjacent prisms Ω_e and Ω_f (lying within a common layer). Two stacked prisms Ω_e and Ω_f share an interior triangular face S_e. A unit normal vector $(\mathbf{n}^e, n_z^e)$ is associated to each of these interior geometric items, with the superscript e indicating that it is oriented from e to f (with $e > f$).

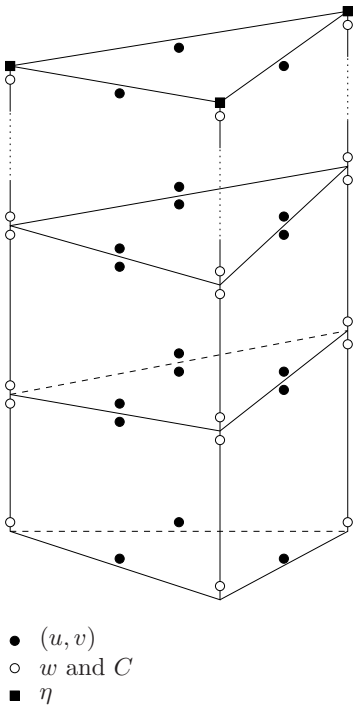

Figure 3: Location of nodes within a column split into prisms. The top triangle is the surface triangle. The free-surface elevation η is linear and continuous. The horizontal velocity is linear non-conforming in the horizontal and linear discontinuous in the vertical (indicated by two nodes sharing a common physical edge). The discontinuous representation in the vertical is particularly well suited for shear regions, as it commonly occurs in baroclinic flows. The vertical velocity and tracers are linear everywhere, yet discontinuous in the vertical.

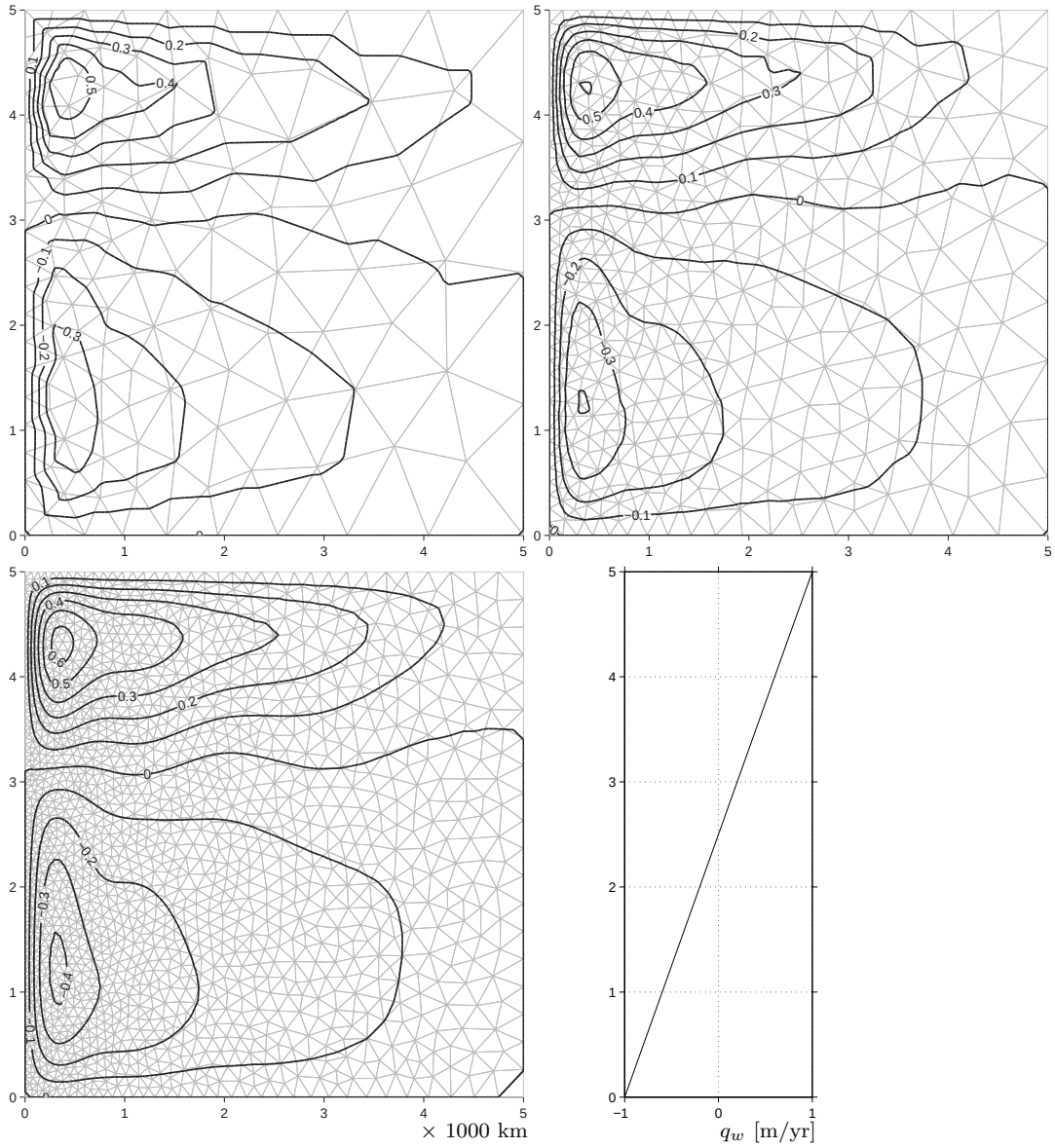

Figure 4: Barotropic streamfunction in Sv (1 Sv = 10^6 m^3/s) for the freshwater-induced Goldsbrough-Stommel circulation on meshes with decreasing element sizes. The freshwater forcing q_w varies linearly in y between -1 and 1 m $year^{-1}$, respectively corresponding to evaporation in the south and precipitation in the north. Numerical experiments are carried out in a square basin of size 5000 km and depth 4000 m. Equations are solved on a β-plane centered at 30°N. The coefficients of horizontal and vertical eddy viscosity are 5×10^4 m^2 s^{-1} and 10^{-4} m^2 s^{-1}, respectively. Meshes are refined along the western boundary of the basin. Resolution varies between 250 and 1000 km for the coarse mesh, between 125 and 500 km for the intermediate mesh and between 62.5 and 250 km for the fine mesh. The coarse mesh contains 215 elements. Upon refinement, the number of elements roughly quadruples.

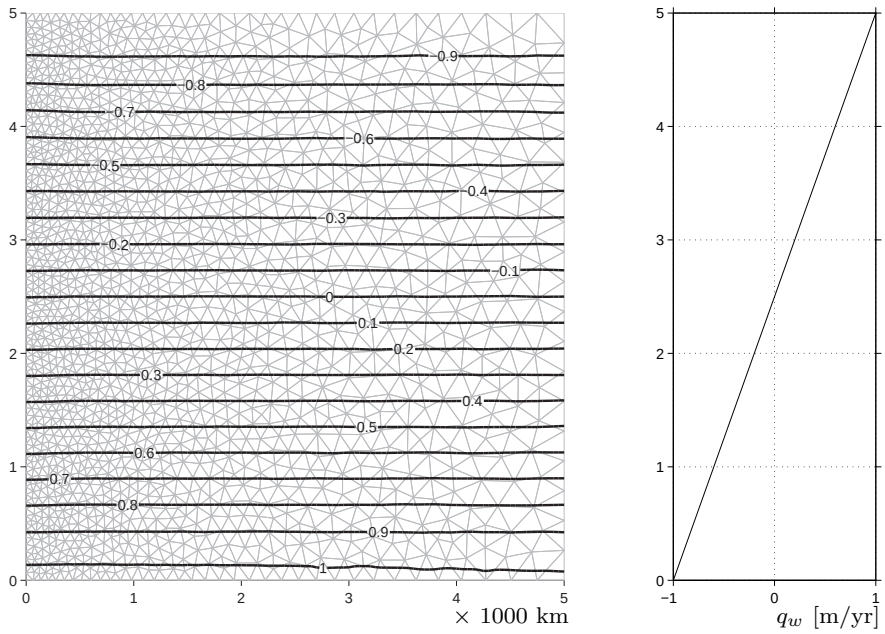

Figure 5: Deviation in psu of surface salinity from the reference value after a three-year run. In this experiment, salinity acts as a passive tracer: it does not feed back the flow. The salinity gradient buildup has the potential of driving a strong baroclinic circulation.

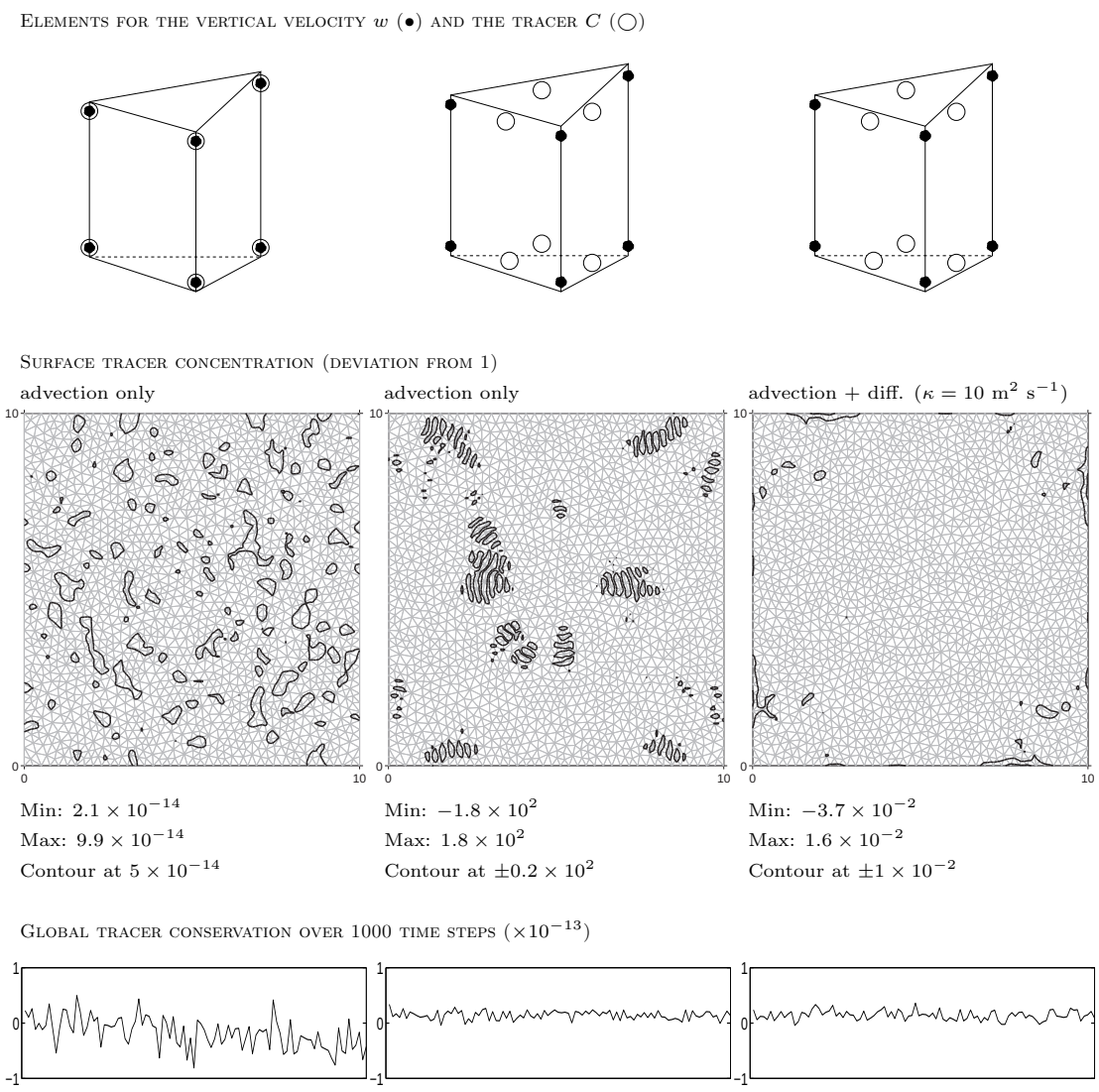

Figure 6: Illustration of consistency breakdown incurred when using different elements for the vertical velocity w and the tracer C. In all simulations, the tracer concentration is initially set to 1 and should remain equal to 1 at all time. The surface flux term (see Eq. 28) is discarded to ensure global conservation in all experiments (see lower panels). The domain is 10 km wide and 20 m deep. The initial elevation field is a 2-meter high Gaussian. The time step is 72 s. We use the P_1 element for the elevation in all runs. The three-dimensional mesh is described and shown in Figure (7). We clearly see that using the same elements for w and C consistently ensures global conservation (surface deviations are zero in machine precision).

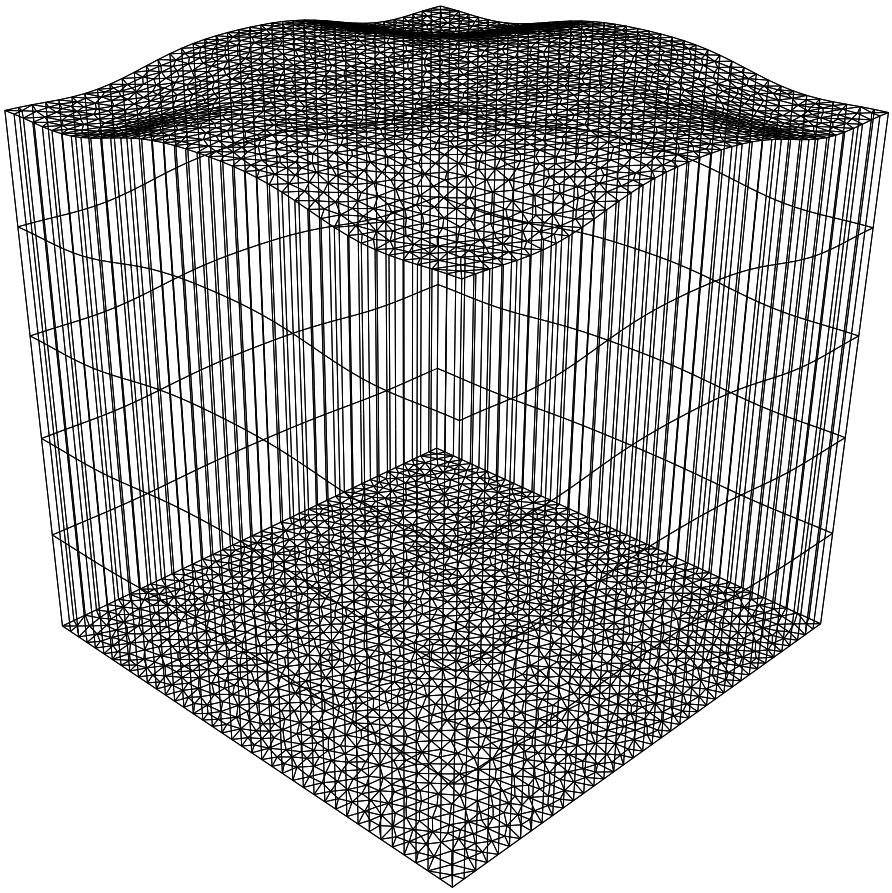

Figure 7: Three-dimensional mesh used for the numerical experiments described in Figure (6). The mesh has a resolution of 250 m in the horizontal and comprises five equally-spaced layers in the vertical. The ratio depth/width has been rescaled for clarity but the ratio of the free-surface elevation to the depth respects the physical dimensions (depth of 20 m and free-surface undulations of the order of 1 m).

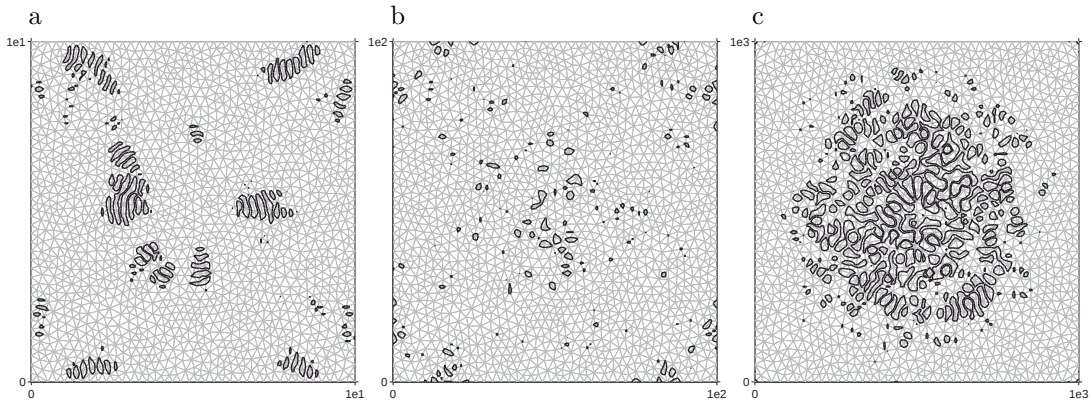

Figure 8: The above panels show the deviation of the tracer concentration at the surface of the domain. The tracer is initially set to 1 throughout the domain and should remain equal to 1 at all time. In all runs, we used the mesh shown in Figure (7). (a) Shelf scale: contour drawn for deviations of -20 and 20 (resolution is 250 m). (b) Intermediate scale: contour drawn for deviations of -0.005 and 0.005 (resolution is 2.5 km). (c) Basin scale: contour drawn for deviations of -0.001 and 0.001 (resolution is 25 km). The corresponding simulation features are given below each panel. The initial elevation field is a 2-meter high Gaussian.